THE JOURNAL OF BIOLOGICAL CHEMISTRY VOL. 281, NO. 41, pp. 30947–30956, October 13, 2006

Targeting Protein Kinase C Activity Reporter to Discrete Intracellular Regions Reveals Spatiotemporal Differences in Agonist-dependent Signaling*

Received for publication, April 19, 2006, and in revised form, August 8, 2006 Published, JBC Papers in Press, August 10, 2006, DOI 10.1074/jbc.M603741200

Lisa L. Gallegos[‡§], **Maya T. Kunkel**[‡], **and Alexandra C. Newton**[‡1]

From the [‡]*Department of Pharmacology and the* [§]*Biomedical Sciences Graduate Program, University of California at San Diego, La Jolla, California 92093*

Protein kinase C (PKC) family members transduce an abundance of diverse intracellular signals. Here we address the role of spatial and temporal segregation in signal specificity by measuring the activity of endogenous PKC at defined intracellular locations in real time in live cells. We targeted a genetically encoded fluorescence resonance energy transfer-based reporter for PKC activity, C kinase activity reporter (CKAR) (Violin, J. D., Zhang, J., Tsien, R. Y., and Newton, A. C. (2003) *J. Cell Biol.* 161, 899–909), to the plasma membrane, Golgi, cytosol, mitochondria, or nucleus by fusing appropriate targeting sequences to the NH_2 or COOH terminus of CKAR. Measuring the phosphorylation of the reporter in the presence of PKC inhibitors, activators, and/or phosphatase inhibitors shows that activity at each region is under differential control by phosphatase activity; nuclear activity is completely suppressed by phosphatases, whereas membrane-associated activity is the least suppressed by phosphatases. UTP stimulation of endogenous P2Y receptors in COS 7 cells reveals spatiotemporally divergent PKC responses. Imaging the second messengers Ca^{2+} and diacylglycerol (DAG) reveal that PKC activity at each location is driven by an initial spike in Ca^{2+}, followed by location-specific diacylglycerol generation. In response to UTP, phosphorylation of GolgiCKAR was sustained the longest, driven by the persistence of DAG, whereas phosphorylation of CytoCKAR was of the shortest duration, driven by high phosphatase activity. Our data reveal that the magnitude and duration of PKC signaling is location-specific and controlled by the level of phosphatase activity and persistence of DAG at each location.

Cells respond dynamically to environmental cues conveyed by complex networks of signal transduction. Phosphorylation is the archetypal language that relays information from environmental stimuli throughout the cell; thus, hundreds of kinases and phosphatases exist to regulate the phosphorylation status of intracellular substrates. A delicate balance of phosphorylation and dephosphorylation underlies cellular decisions ranging from controlling global functions, such as proliferation or apoptosis, to regulating specialized functions, such as secretion of hormones (2, 3). Disturbing this balance can lead to disease states, most notably cancer (4).

The protein kinase C (PKC)[2] family of Ser/Thr kinases transduces an abundance of extracellular signals that control diverse cellular functions, including differentiation, memory, and apoptosis. There are 10 mammalian isozymes of the PKC family, and they share a conserved COOH-terminal kinase core as well as an NH_2-terminal autoinhibitory pseudosubstrate peptide that is lodged in the active site under resting conditions. PKC isoforms are classified into three subcategories (conventional, novel, and atypical) based on differing composition of their regulatory modules, which lie between the kinase core and inhibitory pseudosubstrate peptide (5). Conventional isoforms of PKC (cPKCs; α, βI, βII, and γ) contain a tandem C1 repeat followed by a C2 domain, which allow them to respond to the second messengers diacylglycerol (DAG) and Ca^{2+}, respectively. When extracellular signals stimulate phosphoinositide hydrolysis, DAG is produced and Ca^{2+} is released. The binding of these second messengers to the regulatory domains results in translocation of cPKCs to cellular membranes. Both second messengers must be present for high affinity membrane binding, an event that provides the energy to disengage the inhibitory pseudosubstrate peptide from the active site, allowing downstream signaling (6). Novel isoforms of PKC (nPKCs; δ, ϵ, η, and θ) are similarly activated by membrane binding; however, the novel C2 domain of the nPKCs cannot bind Ca^{2+}. For these isozymes, high affinity membrane binding is achieved exclusively by the C1 domain, which compensates by having an increased affinity for DAG (7). Consequently, this subclass is regulated by DAG production but not by Ca^{2+} release. Atypical PKCs ζ and ι are unique in that they are not regulated by either DAG or Ca^{2+}; their regulatory region consists of an atypical C1 domain that does not bind DAG and a PB1 (Phox and Bem 1) domain, recently recognized for its role in protein-protein interactions (8). Since activation of receptors can result in different profiles of Ca^{2+} release and DAG production, PKC isoforms are poised to

* This work was supported by National Institutes of Health Grants P01 DK54441 and GM-43154. The costs of publication of this article were defrayed in part by the payment of page charges. This article must therefore be hereby marked "*advertisement*" in accordance with 18 U.S.C. Section 1734 solely to indicate this fact.

[1] To whom correspondence should be addressed: Dept. of Pharmacology, University of California at San Diego, 9500 Gilman Dr. 0721, La Jolla, CA 92039-0721. Tel.: 858-534-4527; Fax: 858-822-5888; E-mail: anewton@ucsd.edu.

[2] The abbreviations used are: PKC, protein kinase C; cPKC, conventional PKC; nPKC, novel PKC; DAG, diacylglycerol; FRET, fluorescence resonance energy transfer; CKAR, C kinase activity reporter; CFP, cyan fluorescent protein; YFP, yellow fluorescent protein; PDBu, phorbol 12,13-dibutyrate; DBD, DAG binding domain; DAGR, DAG reporter; BAPTA, 1,2-bis(2-aminophenoxy)ethane-*N*,*N*,*N*′,*N*′-tetraacetic acid; PLC, phospholipase C.

respond to receptor activation with varying magnitude and duration of activity (9).

Previously, our laboratory generated a genetically encoded fluorescence resonance energy transfer (FRET)-based reporter for PKC activity (1). C kinase activity reporter (CKAR) is composed of a cyan fluorescent protein (CFP) and yellow fluorescent protein (YFP) tethered together by a substrate peptide specific for PKC and an FHA2 phosphopeptide-binding module. When CKAR is not phosphorylated, excitation at the characteristic CFP wavelength (434 nm) results in FRET, and YFP emission (528 nm) is observed. When PKC phosphorylates the substrate sequence, the FHA2 domain binds the phosphopeptide, reducing the energy transfer and increasing CFP emission (476 nm). A ratio of CFP/FRET emission provides a readout of the phosphorylation state of the population of reporters in the cell. The affinity of the phosphopeptide for the phosphopeptide-binding module is sufficiently high to trigger intramolecular binding but, importantly, is also in a range that allows for access of the phospho-substrate to cellular phosphatases. Thus, CKAR is sensitive to dephosphorylation and provides a reversible, real time readout of the balance between PKC and phosphatase activity. Importantly, CKAR is an assay of endogenous PKC activity from live, intact cells and retains any potential inputs from other key cellular partners, such as protein and lipid regulatory factors.

Although the plasma membrane has historically been considered the site of action of PKCs, several studies have demonstrated PKC translocation to the Golgi, mitochondria, and the nucleus in response to different stimuli (7, 10–12). However, mechanisms controlling the differential regulation of PKC activity, the balance between phosphatase and kinase activity, and the duration of signaling at these locations are not known.

In this study, we targeted CKAR to the plasma membrane, Golgi, mitochondria, cytosol, and nucleus and characterized activity of PKC at each region in response to stimulation. We used a specific inhibitor of conventional PKCs, Gö6976, to measure basal PKC activity; the potent DAG mimic, PDBu, to measure stimulated PKC activity; and the phosphatase inhibitor, calyculin A, to measure phosphatase-suppressed PKC activity. Stimulation of endogenous P2Y G protein-coupled receptors with UTP in COS 7 cells revealed regionally divergent PKC responses. We investigated the underlying basis for phosphorylation profiles in COS 7 cells at each intracellular localization by imaging Ca^{2+} release and localized DAG production in response to UTP. We discovered that the early phase of the PKC response is governed by Ca^{2+} release, whereas the later phase of the PKC response is controlled by localized DAG persistence. Unexpectedly, in COS 7 cells, DAG production and the corresponding PKC response to UTP are highly sustained at the Golgi compared with the plasma membrane.

MATERIALS AND METHODS

Construction of Targeted Reporters—CKAR was generated previously in the mammalian expression vector pcDNA3 (+) (Invitrogen) (1). The construct contains CFP and YFP tethered together by an FHA2 phosphopeptide binding domain followed by a PKC-specific substrate peptide. PMCKAR was created previously (MyrPalm-CKAR) (1) by the addition of sequences encoding the amino-terminal 7 amino acids of Lyn kinase to the 5′-end of CKAR. GolgiCKAR and MitoCKAR were generated by fusing in frame sequences encoding the amino-terminal 33 amino acids of endothelial nitric-oxide synthase and the amino-terminal 33 amino acids of TOM 20, respectively, to the immediate 5′-end of CKAR (13–15). CytoCKAR was generated by fusing a region encoding the nuclear export sequence, LALKLAGLDI, to the 3′-end of CKAR immediately preceding the termination codon (16). NucCKAR was generated similarly by fusing to the 3′-end of CKAR sequences encoding a basic nuclear localization signal, PKKRKVEDA (17).

Construction of Other Plasmids—Diacylglycerol reporter (DAGR) was constructed as previously described (1). PMCFP was constructed as previously described (1); the amino-terminal 7 residues of Lyn kinase were attached to the 5′-end of monomeric CFP. GolgiCFP was constructed similar to GolgiCKAR; sequences encoding the amino-terminal 33 residues of endothelial nitric-oxide synthase were fused in frame to the 5′-end of CFP (13). YFP-tagged DAG binding domain (YFP-DBD) was first constructed by fusion of monomeric YFP to the 5′-end of the C1b domain of PKCβ. This construct was improved for DAG binding by introducing the Y123W point mutation via QuikChange (Stratagene).

Cell Culture—COS 7 cells were used in all experiments. These cells were plated and maintained in Dulbecco's modified Eagle's medium (Cellgro) containing 10% fetal bovine serum and 1% penicillin/streptomycin at 37 °C in 5% CO_2. Cells were plated in sterilized 35-mm imaging dishes at 60% confluence and transfected using FuGENE 6 (Roche Applied Science). For DAGR imaging experiments, cells were cotransfected with PMCFP and YFP-DBD (PMDAGR) or GolgiCFP and YFP-DBD (GolgiDAGR). Cells were allowed to grow posttransfection for 12–24 h before imaging. For Ca^{2+} imaging experiments, 1.0 μM Fura-2/AM (Molecular Probes, Inc., Eugene, OR) was loaded into cells for 30 min, and cells were washed twice with Hanks' balanced salt solution (Cellgro) before imaging.

Cell Imaging—COS 7 cells were rinsed once with and imaged in Hanks' balanced salt solution containing 1 mM Ca^{2+}. For imaging in Ca^{2+}-free saline, cells were rinsed once with and imaged in Hanks' balanced salt solution containing 5 mM EGTA. Images were acquired on a Zeiss Axiovert microscope (Carl Zeiss Microimaging, Inc.) using a MicroMax digital camera (Roper-Princeton Instruments) controlled by MetaFluor software (Universal Imaging, Corp.). Optical filters were obtained from Chroma Technologies. Using a 10% neutral density filter, CFP and FRET images were obtained every 10–15 s through a 420/20-nm excitation filter, a 450-nm dichroic mirror, and a 475/40-nm emission filter (CFP) or 535/25-nm emission filter (FRET). YFP emission was also monitored as a control for photobleaching through a 495/10-nm excitation filter, a 505-nm dichroic mirror, and a 535/25-nm emission filter. Images of cells loaded with Fura-2 were obtained every 10 s through a 380/10-nm or 340/10-nm excitation filter, a 450-nm dichroic mirror, and a 535/45-nm emission filter. Excitation and emission filters were switched in filter wheels (Lambda 10-2; Sutter). Integration times were 200 ms for CFP, FRET, and Fura-2 and 50–100 ms for YFP.

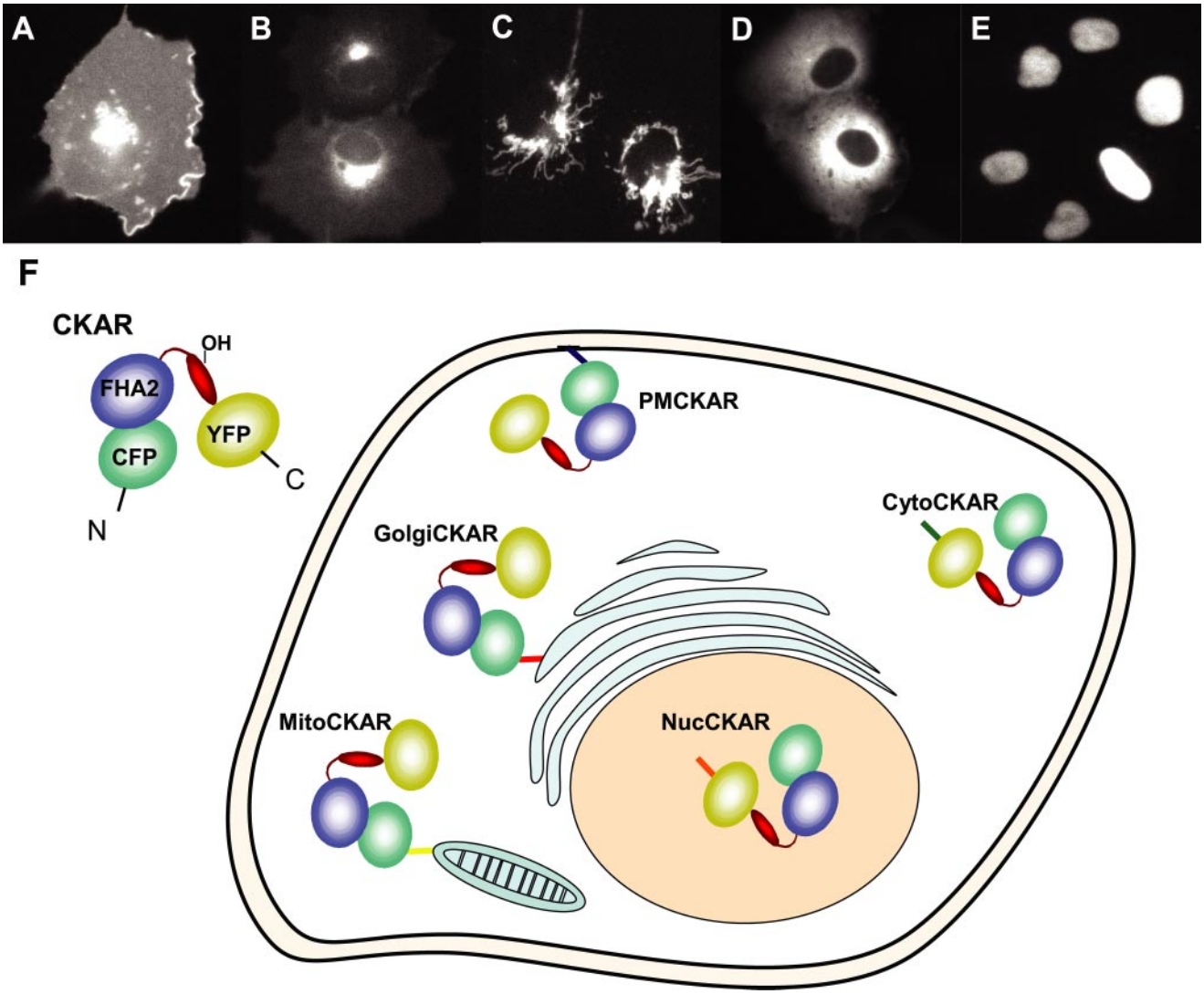

FIGURE 1. **Targeting CKAR.** CKAR, composed of CFP and YFP flanking a substrate sequence specific for PKC and an FHA2 phosphopeptide binding module, can be targeted to different intracellular locations by fusing short targeting motifs to the amino or carboxyl terminus. *A*, CKAR was targeted to the plasma membrane by fusion of the amino-terminal 7 residues of Lyn kinase. *B*, Golgi targeting was achieved by fusion of the amino-terminal 33 residues of endothelial nitric-oxide synthase. *C*, CytoCKAR was generated by COOH-terminal fusion of a hydrophobic sequence for nuclear export. *D*, CKAR was targeted to the outer membrane of the mitochondria by fusion of the amino-terminal 33 residues of TOM20. *E*, fusion of a basic nuclear localization sequence to the COOH terminus targeted CKAR to the nucleus. *F*, schematic representation of targeted CKARs.

Imaging Data Analysis—Images were reanalyzed using Metaflour Analyst (Universal Imaging Corp.). One region per cell was selected such that there was no net movement of the targeted reporter in and out of the selected region, and Metafluor Analyst was used to calculate the average FRET ratio within the selected region as described previously (1). Base-line images were acquired for 15–30 min before adding ligand. In some cases, there was a base-line drift that accounted for up to a 7% change in maximal FRET ratio per 10 min. This base line was subtracted from traces. The corrected data traces were normalized to 1 by dividing by the average base-line FRET ratio, and data from different imaging dishes were referenced around the ligand addition time point. The normalized average FRET ratio is the average of these corrected values ± S.E.

RESULTS

Targeted CKARs—To monitor PKC activity at defined intracellular locations, we fused short sequences to the amino or carboxyl terminus of the reporter that drive specific intracellular localization. The fluorescent images in Fig. 1 show the subcellular localization of the targeted CKAR constructs expressed in COS 7 cells. PMCKAR (Fig. 1*A*) contains the NH_2-terminal 7 residues of Lyn kinase fused in frame before CFP, effectively targeting it to the plasma membrane via myristoylation and palmitoylation (1). GolgiCKAR (Fig. 1*B*) was targeted to the cytoplasmic face of the Golgi apparatus by attaching the NH_2-terminal 33 residues of endothelial nitric-oxide synthase (13, 15). CytoCKAR (Fig. 1*C*) was excluded from the nucleus by COOH-terminal fusion of a hydrophobic sequence for nuclear export (16) and MitoCKAR (Fig. 1*D*) was targeted to the outer mitochondrial membrane by fusion of the NH_2-terminal 33 residues of TOM 20 (14). NucCKAR (Fig. 1*E*) was localized to the nucleus by COOH-terminal fusion of a basic nuclear localization sequence (17). Fig. 1*F* shows a schematic representation of the localization of the tethered CKARs. To verify

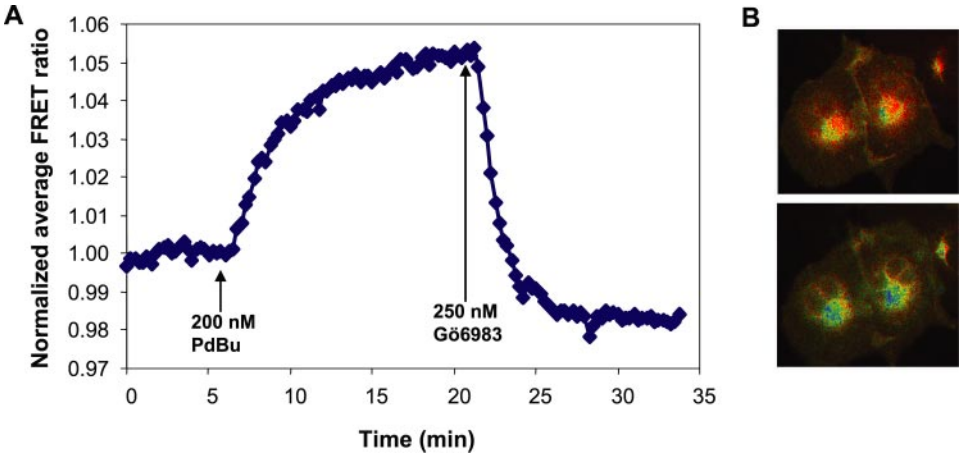

FIGURE 2. **Targeted CKAR retains specificity and reversibility in monitoring PKC activity in live cells.** *A*, COS 7 cells were transfected with GolgiCKAR, and the FRET ratio was quantified following the addition of PDBu (200 nM) and then the specific PKC inhibitor Gö6983 (250 nM). *B*, images corresponding to data in *A* show phosphorylation (red shift of pseudocolored FRET ratio image; *top*) of CKAR after PDBu treatment (15 min time point) and dephosphorylation (blue shift of pseudocolored FRET ratio image; *bottom*) after Gö6983 addition (30 min time point). Data are representative of three independent experiments.

proper targeting of GolgiCKAR and MitoCKAR, we stained cells transfected with the reporters using Golgi-specific tracker dye, BODIPY TR C_5 ceramide, and with mitochondria-specific tracker dye, Deep Red-Fluorescent MitoTracker® (Invitrogen). The reporters completely co-localized with dyes specific for their respective cellular compartment (data not shown). Note that the juxtanuclear concentration of GolgiCKAR was dispersed in the presence of the Golgi-fragmenting agent, Brefeldin A; we also observed a minimal juxtanuclear concentration of PMCKAR, and this was insensitive to brefeldin A (data not shown), suggesting that the apparent juxtanuclear concentration of PMCKAR was in a region distinct from Golgi.

The specificity and reversibility of phosphorylation was tested for each targeted reporter by addressing the sensitivity to activation by phorbol esters and inhibition by a PKC-specific inhibitor. Fig. 2 shows that PDBu treatment of COS 7 cells triggered an increase in FRET ratio of GolgiCKAR, revealing robust activity of endogenous PKC at this location. This phosphorylation was reversed with the addition of the specific PKC inhibitor, Gö6983. Similar phorbol ester-dependent and inhibitor-reversed phosphorylation was noted for each targeted CKAR (data not shown).

Dynamic Range of Targeted CKARs—Phorbol esters, potent functional analogs of DAG, are the classic tool for activating PKC in cells (18). We first determined the kinetics and magnitude of the stimulated PKC response at each cellular region as a consequence of PDBu treatment. Fig. 3*A* shows the change in FRET ratio following PDBu stimulation of COS 7 cells expressing either PMCKAR, GolgiCKAR, CytoCKAR, MitoCKAR, or NucCKAR. The fastest response was observed at the plasma membrane ($t_{½} \approx 0.6$ min), followed by Golgi ($t_{½} \approx 2.7$ min), mitochondria ($t_{½} \approx 4$ min), and cytosol ($t_{½} \approx 7$ min). These differences did not simply reflect the rate of PDBu partitioning, since the isolated C1b domain from PKCβ translocated to membranes throughout the cell within 0.5 min of PDBu addition (data not shown). No PDBu-stimulated activity was observed in the nucleus. The highest magnitude of the response was at the Golgi. Although the initial FRET ratios varied, the normalized traces were highly consistent in rate and magnitude and were characteristic to each region.

Reversal of PDBu-stimulated activity by inhibition of PKC typically resulted in a decrease in reporter phosphorylation below base line (Fig. 2*A*), leading us to hypothesize that the differences in PDBu-stimulated activity might result from differing levels of basal PKC activity at each region. Thus, after acquiring base-line images, we measured the effect of treating cells with the conventional PKC inhibitor Gö6976 as a measure of the basal PKC activity (Fig. 3*B*). Although Gö6983 specifically inhibits all isoforms of PKC, it could not be used to characterize the basal activity, because it emits at a wavelength that is visible in the FRET channel and partitions unequally within the cell (data not shown). The highest basal activity was at the plasma membrane. GolgiCKAR and CytoCKAR were also basally phosphorylated, whereas NucCKAR and MitoCKAR responded minimally to inhibition of basal PKC activity with Gö6976. Thus, basal PKC activity in unstimulated cells varies dramatically depending on the cellular region.

Another component of the localized PKC response is the opposition to substrate phosphorylation by regional phosphatases. We reasoned that the basis for low basal and stimulated activity in some areas may be potent signal termination by local phosphatases. To test this hypothesis, we first stimulated PKC with PDBu and allowed phosphorylation to reach a steady state. Once the response leveled, we added the broad spectrum phosphatase inhibitor, calyculin A, to release phosphatase suppression (Fig. 3*C*). Inhibition of phosphatases resulted in a robust phosphorylation of nuclear CKAR and, to a lesser extent, cytosolic CKAR. Membrane-tethered CKAR was much less sensitive to phosphatase inhibition, particularly at the plasma membrane, where the prior treatment with phorbol esters had resulted in maximal CKAR phosphorylation. Interestingly, even in the absence of PDBu, inhibition of phosphatase activity with calyculin A was sufficient to induce phosphorylation of CKAR at each region (Fig. 3*D*). The increase in CKAR phosphorylation upon treatment with calyculin A was a specific effect of releasing PKC inhibition, since it was blocked with Gö6983.[3] These data reveal that PKC activity is antagonized by phosphatases to varying degrees depending on the enzyme's cellular location.

Assembling the components of the PKC response at each region into a bar graph revealed that the sum of basal, stimulated, and phosphatase-suppressed PKC activity was similar at all intracellular regions, with the exception of MitoCKAR,

[3] J. Violin, unpublished results.

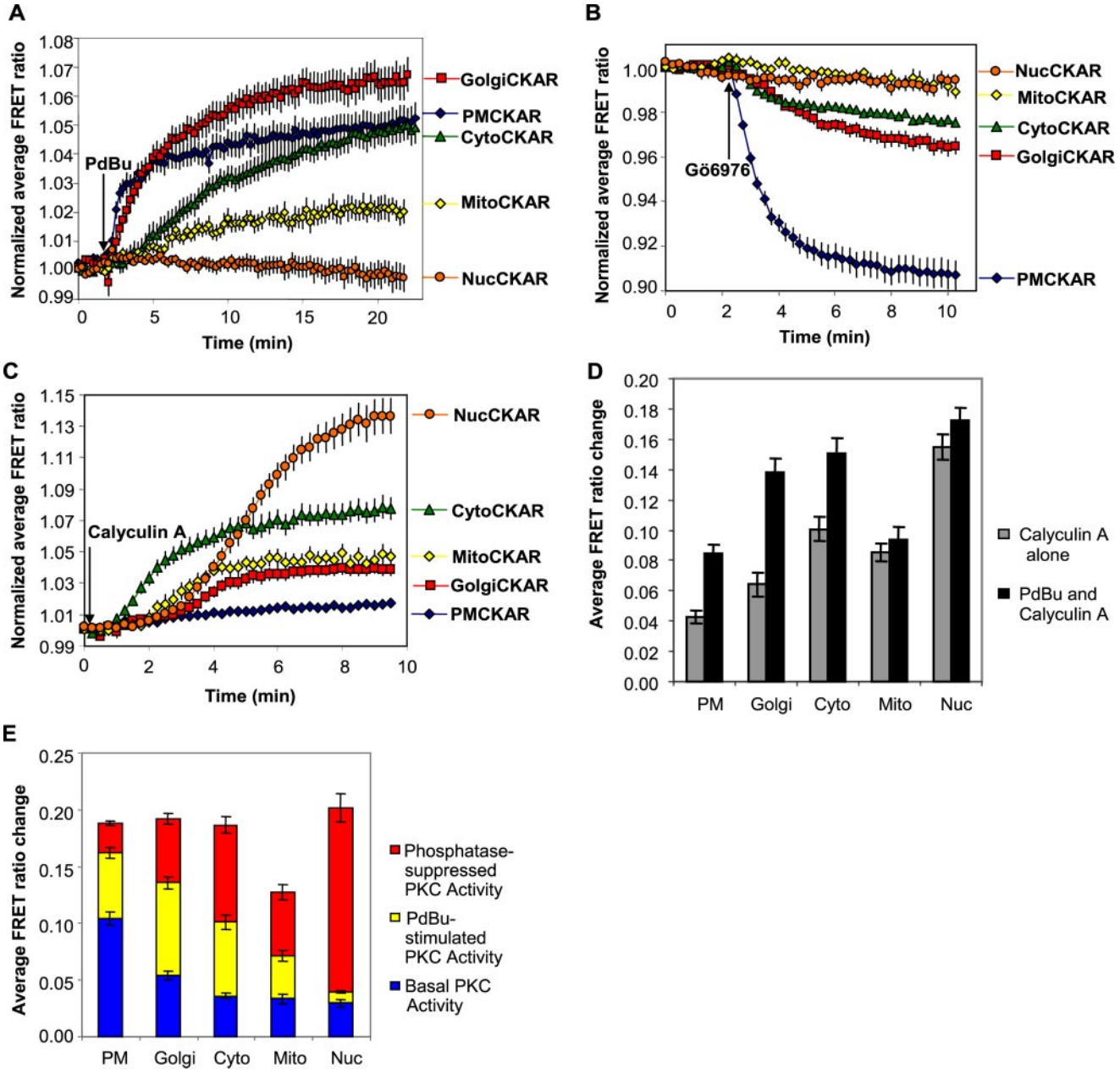

FIGURE 3. **Localized PKC activity in COS 7 cells.** *A*, COS 7 cells were transfected with the indicated targeted constructs of CKAR, and the average FRET ratio was quantified as a function of time following PDBu (200 nM) treatment: GolgiCKAR (*red squares*), PMCKAR (*blue diamonds*), CytoCKAR (*green triangles*), MitoCKAR (*yellow diamonds*), and NucCKAR (*orange circles*). These data reveal the magnitude of the phorbol ester-stimulated response. *B*, COS 7 cells were transfected with targeted CKAR constructs and the FRET ratio monitored following treatment with Gö6976 (500 nM), an inhibitor of conventional isoforms of PKC. These data reveal the magnitude of the basal conventional PKC activity at each location. *C*, COS 7 cells transfected with various CKAR constructs were stimulated with PDBu (200 nM) for 20 min until the maximal phorbol ester stimulation was achieved. At this point, the FRET ratio was measured before and after the addition of calyculin A (50 μM) to inhibit cellular phosphatases. The magnitude of the calyculin A-stimulated response reveals the phosphatase-suppressed PKC activity at each region. *D*, COS 7 cells transfected with the various CKAR constructs were stimulated with PDBu (200 nM) and calyculin A (50 μM) (*black bars*) or calyculin A (50 μM) alone (*gray bars*). *E*, quantitation of the basal, stimulated, and phosphatase-suppressed PKC activities at specific regions, showing the range of CKAR at each cellular location. Data represent the average ± S.E. of 10–25 cells from at least three independent experiments referenced around the addition time point.

which had about two-thirds the range of an untethered reporter (Fig. 3*E*). Further analysis revealed that the mitochondrial reporter, unlike all of the others, becomes partially cleaved within CFP when expressed in mammalian cells (data not shown). Thus, with the exception of MitoCKAR, the range of the reporters was not affected by targeting, thus allowing accurate comparison of responses following stimulation of endogenous signaling pathways. Furthermore, this characterization reveals that the subsequent data showing phosphorylation of the targeted CKARs in response to the G protein-coupled receptor ligand, UTP, is not limited by reporter saturation.

Localized PKC Responses to Stimulation of Endogenous Receptors—We next addressed the profile of regional phosphorylation triggered by receptor-mediated stimulation. UTP initiates a PKC response by activating G_q-coupled P2Y receptors on the surface of epithelial cells, producing the second messengers DAG and inositol trisphosphate, which stimulates intracellular Ca^{2+} release (19, 20). Fig. 4 summarizes targeted CKAR

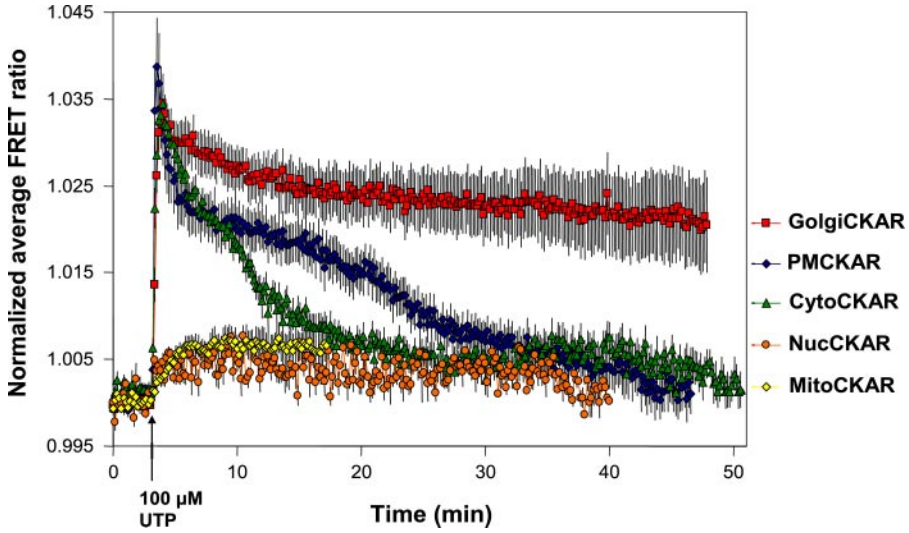

FIGURE 4. **PKC response to UTP in COS 7 cells.** COS7 cells transfected with the indicated targeted CKARs were treated with UTP (100 μM), and the FRET ratio was visualized as a function of time. Data shown are an average ± S.E. of 11–16 cells from three independent experiments referenced around the ligand addition time point.

phosphorylation in COS 7 cells in response to UTP. PMCKAR, GolgiCKAR, and CytoCKAR were rapidly phosphorylated, with an early crest (peaking within 1 min) followed by a late sustained plateau. Phosphorylation on CytoCKAR was most readily reversed back to base line, consistent with higher phosphatase sensitivity of CytoCKAR. Phosphorylation on GolgiCKAR was sustained throughout the course of the experiment, whereas PMCKAR was dephosphorylated to base line within 35 min. MitoCKAR and NucCKAR were not readily phosphorylated in response to UTP.

Second Messenger Responses—We next examined the underlying causes for the biphasic nature of the PKC response to UTP. Specifically, we asked how CKAR phosphorylation correlated with production of Ca^{2+} and DAG. First, we monitored Ca^{2+} release downstream of receptor stimulation using the Ca^{2+}-sensitive fluorescent probe, Fura-2 (21). Fig. 5*A* reveals the temporal relationship between Ca^{2+} release and the early phase of the PKC response at the Golgi and plasma membrane. Upon the addition of UTP, a transient wave of Ca^{2+} was released that corresponded with the early phase of PKC activity. To confirm that this early phase of PKC activity is driven by Ca^{2+}, we monitored phosphorylation in response to UTP after pretreatment with BAPTA to chelate intracellular Ca^{2+} (22). Chelation of Ca^{2+} abolished the early peak in PKC activity both at the plasma membrane (Fig. 5*B*) and at the Golgi (Fig. 5*C*). These data reveal that Ca^{2+} is required for the initial peak in PKC activity following UTP stimulation.

The rate of PMCKAR phosphorylation ($t_{½} \approx 0.2$ min) was significantly reduced in the presence of BAPTA ($t_{½} \approx 1.2$ min). The rate of GolgiCKAR phosphorylation in the presence of BAPTA was also reduced, although only modestly. This reduction could arise because novel PKCs are activated at a slower rate than conventional PKCs or because the lower level of novel PKCs compared with conventional PKCs in COS cells results in slower kinetics of CKAR phosphorylation. Alternatively, the diminished activity in the presence of BAPTA could represent partial activation of conventional PKCs, with the C1 domain participating in activation by binding DAG but the C2 domain refraining from providing the extra energy to fully disengage the pseudosubstrate. To address whether the slower phosphorylation catalyzed by endogenous novel PKCs (*i.e.* in the presence of BAPTA) reflected subsaturating concentrations of these kinases, we transfected in PKCδ, a novel isoform, to attempt to rescue the fast kinetics of phosphorylation in response to UTP. To ensure the residual activity was not due to partial activation of cPKCs, we also added the conventional PKC inhibitor, Gö6976. Gö6976 did not block the response, and, although the response was slightly faster with overexpressed PKCδ (as a result of higher total PKC expression), the fast phase of the PKC response was not restored (Fig. 5, *B* and *C*). Therefore, Ca^{2+}-responsive cPKCs are responsible for the fast, early phase of the PKC response whereas nPKCs account for the slow, later phase of the PKC response.

Because Ca^{2+} release was necessary for the fast phase of PKC activation, we tested if calcium release alone was sufficient for activation of cPKCs. To uncouple Ca^{2+} release from DAG production, we stimulated COS 7 cells with UTP in the absence of extracellular calcium and in the presence of cell-impermeant Ca^{2+} chelator, EGTA. This allows Ca^{2+} release from intracellular stores, resulting in a sharp peak of calcium release (Fig. 5*D*), but does not allow calcium-induced calcium release. Under these conditions, no overall DAG increase occurred, as monitored by the intermolecular FRET-based DAGR (Fig. 5*E*, *gray triangles*) (1). Importantly, with Ca^{2+} release alone, no phosphorylation of PMCKAR or GolgiCKAR occurred (Fig. 5*E*).

Because the Ca^{2+} release terminated well before reporter dephosphorylation, we tested whether the persistence of the PKC response correlated with the other upstream second messenger, DAG. Specifically, phosphorylation of PMCKAR was reversed within 35 min, but GolgiCKAR remained phosphorylated throughout the course of the experiment (Fig. 4). In order to examine local DAG levels, we cotransfected a YFP-tagged DAG binding domain (YFP-DBD) with either PMCFP (PM DAG reporter, or PMDAGR) or GolgiCFP (Golgi DAG reporter, or GolgiDAGR) and watched a stimulated increase in the ratio of FRET/CFP emission (FRET ratio) as the DBD translocated from the cytosol to the plasma and Golgi membranes (Fig. 6*A*). The DBD consists of the C1b domain from PKCβ containing a recently discovered single point mutation (Y123W) that increases the affinity of the C1b domain for DAG.[4] Fig. 6*B* shows that upon the addition of UTP, DAG was produced at both the plasma and Golgi mem-

[4] D. Dries, L. Gallegos, and A. Newton, manuscript in preparation.

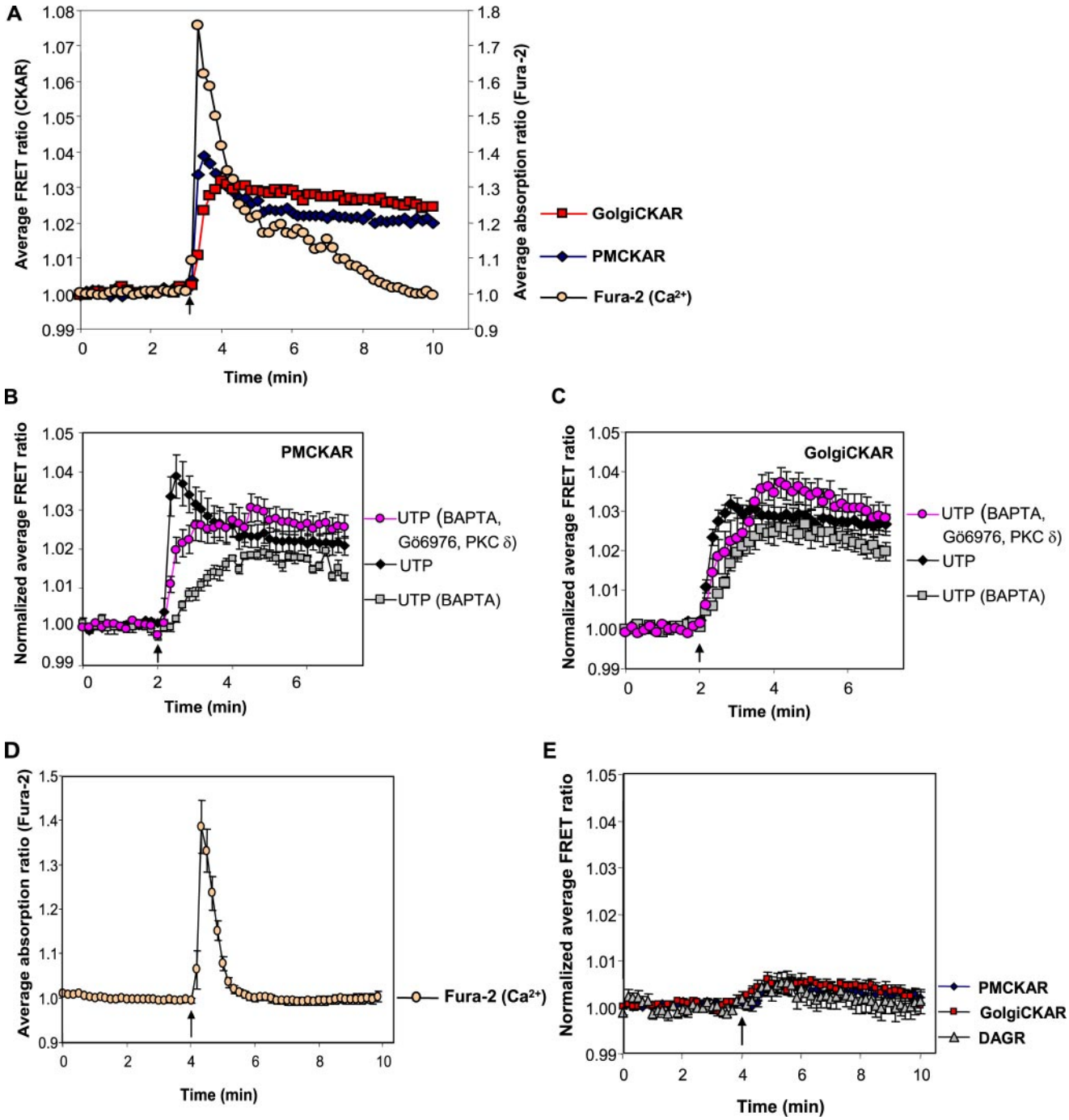

FIGURE 5. **Ca^{2+} release is responsible for early phase of the UTP-stimulated PKC response.** *A*, COS 7 cells loaded with Fura-2 were imaged after stimulation with UTP (100 μM) at 3 min (*black arrow*). Fura-2 absorption ratio (340/380 nm) monitors Ca^{2+} release (*tan circle*). PMCKAR (*blue diamonds*) and GolgiCKAR (*red squares*) responses to UTP (100 μM) were scaled and overlaid on the plot to show temporal correlation. *B*, COS 7 cells were transfected with PMCKAR alone (*black diamonds*, *gray squares*) or PMCKAR and PKCδ (*pink circles*). Cells were then stimulated with UTP (100 μM; *black diamonds*) or pretreated with BAPTA (15 min, 15 μM) and then stimulated with UTP (100 μM; *gray squares*) or pretreated with both BAPTA (15 μM) and Gö6976 (500 nM) and then stimulated with UTP (100 μM; *pink circles*). The *black arrow* shows UTP added at 2 min. *C*, COS 7 cells were transfected with GolgiCKAR alone (*black diamonds*, *gray squares*) or GolgiCKAR and PKCδ (*pink circles*). Cells were then stimulated with UTP (100 μM; *black diamonds*) or pretreated with BAPTA (15 min, 15 μM) and then stimulated with UTP (100 μM; *gray squares*) or pretreated with both BAPTA (15 μM) and Gö6976 (500 nM) and then stimulated with UTP (100 μM; *pink circles*). The *black arrow* shows UTP added at 2 min. *D*, COS 7 cells were loaded with Fura-2 and imaged in Ca^{2+}-free saline and EGTA (5 mM) after stimulation with UTP (100 μM) at 4 min (*black arrow*). Fura-2 absorption ratio (340/380 nm) monitors Ca^{2+} release (*tan circles*). *E*, COS 7 cells were transfected with DAGR to monitor global DAG production (*gray triangles*), PMCKAR (*blue diamonds*), or GolgiCKAR (*red squares*) and imaged in Ca^{2+}-free saline and EGTA (5 mM) after stimulation with UTP (100 μM) at 4 min (*black arrow*). Data represent the average ± S.E. of 10–25 cells from at least three independent experiments referenced around the addition time point.

branes. However, whereas the FRET ratio increase from PMDAGR reversed within 40 min, the FRET ratio increase from GolgiDAGR was sustained throughout the course of the experiment. Thus, UTP caused differential duration of the DAG signal at the plasma membrane and Golgi, setting the duration of CKAR phosphorylation at each location.

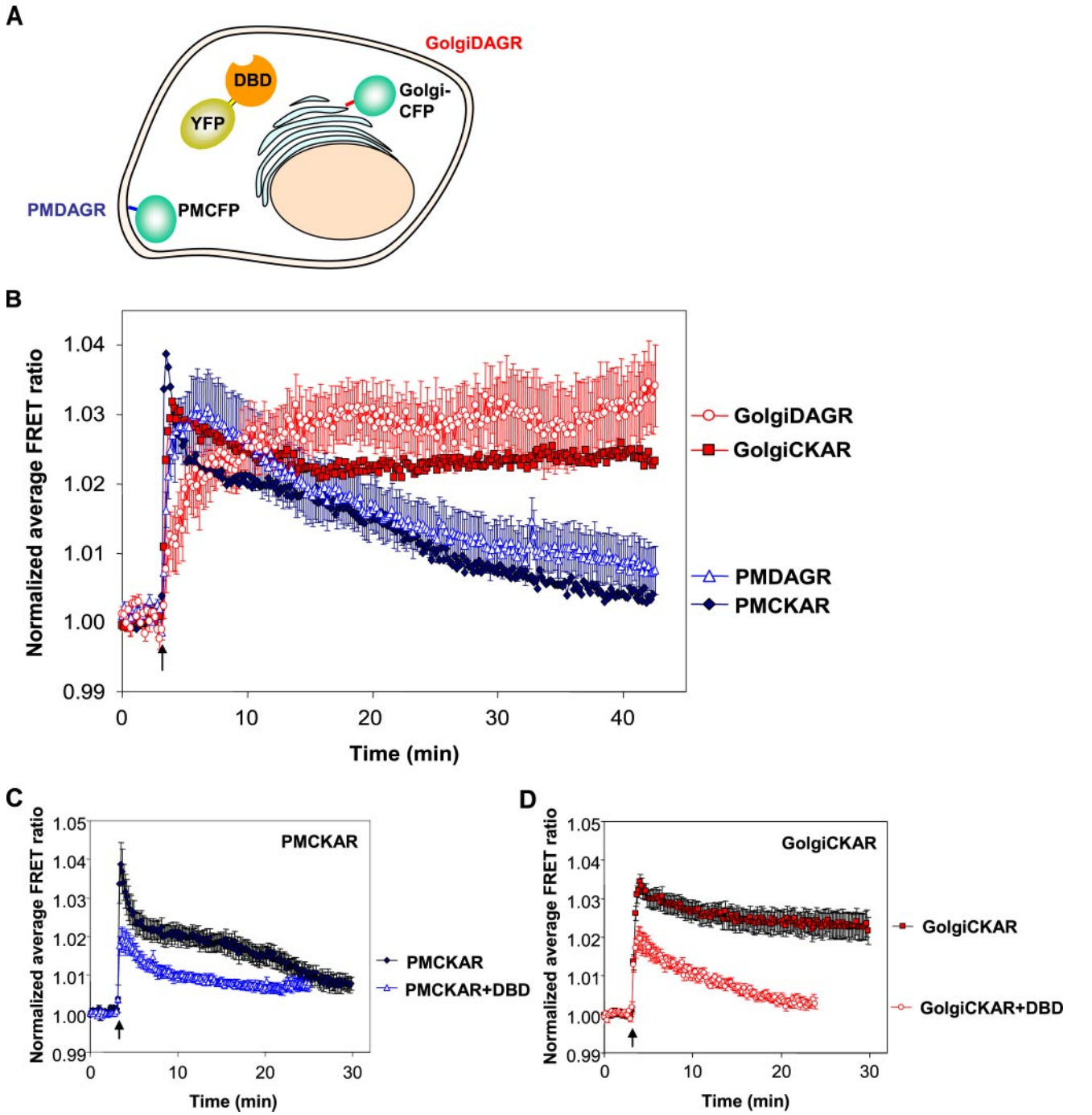

FIGURE 6. **Localized persistence in PKC activity follows DAG persistence.** *A*, schematic representaion of PMDAGR and GolgiDAGR system. *B*, COS 7 cells cotransfected with YFP-DBD and PM-CFP (PMDAGR; *open blue triangles*) or YFP-DBD and Golgi-CFP (GolgiDAGR, *open red circles*) were stimulated with UTP (100 μM) at 3 min (*black arrow*). Localized DAGR responses were plotted together with PMCKAR (*closed blue diamonds*) and GolgiCKAR (*closed red squares*) responses to UTP (100 μM) to show temporal correlation. *C*, COS 7 cells transfected with PMCKAR (*blue diamonds*) or PMCKAR and DBD (*open blue triangles*) were stimulated with UTP (100 μM) at 3 min (*black arrow*). *D*, COS 7 cells transfected with GolgiCKAR (*red squares*) or GolgiCKAR and DBD (*open red circles*) were stimulated with UTP (100 μM) at 3 min (*black arrow*). CKAR and DAGR responses derive from an average of 15–25 cells from three independent experiments, referenced around the ligand addition time point.

To further examine the contribution of DAG to the late phase of the PKC response, we next tested whether excess DBD would competitively block DAG-dependent PKC activation. We cotransfected untagged DBD with PMCKAR (Fig. 6*C*) or GolgiCKAR (Fig. 6*D*) and monitored phosphorylation in response to UTP treatment. We found that the DBD did not completely block the fast phase of the PKC response in either region but caused shorter duration of phosphorylation in both regions.

DISCUSSION

We have dissected the PKC response at distinct subcellular locations by targeting CKAR, a genetically encoded FRET-based PKC activity reporter, to specific locations within the cell.

Imaging the reporter following stimulation of endogenous P2Y receptors in COS 7 cells revealed biphasic responses in phosphorylation that were characteristic to each region. We show that the magnitude and duration of responses at each location are controlled by Ca^{2+} release, localized DAG production, and the level of phosphatase activity at each site.

CKAR was successfully targeted to the plasma membrane, Golgi, mitochondria, cytosol, and nucleus. Each reporter revealed different basal, stimulated, and phosphatase-suppressed activity, whereas the dynamic range of responses was similar at all locations. Even taking into consideration the possibility of incomplete targeting, the reporters are undeniably enriched in the regions targeted, resulting in distinct phosphorylation profiles among the different regions.

Phosphorylation of PMCKAR was basally elevated and rapidly increased in the presence of PDBu, which highlights the responsiveness of the plasma membrane to external signaling. PDBu caused the greatest increase in phosphorylation of GolgiCKAR, indicating a high capacity for stimulated changes in PKC activity at the Golgi. Membrane-tethered reporters, in general, were much less sensitive to phosphatases than untethered reporters, allowing these substrates a fuller range of responses to stimulation. Strikingly, phosphatase suppression was both necessary and sufficient to allow phosphorylation of NucCKAR. It is possible that provoking a PKC response in the nucleus depends upon coincident inhibition of phosphatase activity rather than the presence of second messengers. Additionally, simply inhibiting phosphatase activity at any region of the cell increased CKAR phosphorylation, which underscores the importance of phosphatases in regulating PKC activity. The targeted CKARs probably serve as faithful representatives of natural PKC substrates and can be useful tools to provide information about the cellular environment surrounding PKC substrates that are localized in different regions of the cell for any period of time.

UTP stimulates G_q-coupled P2Y receptors in epithelial cells (19, 20) which, in COS 7 cells, generates a spike of Ca^{2+} release as well as production of DAG via phospholipase C (PLC)-mediated lipid hydrolysis. We were able to detect an early peak of PKC activity on PMCKAR, GolgiCKAR, and CytoCKAR that correlated temporally with Ca^{2+} release. By buffering intracellular Ca^{2+} with BAPTA, the early peak of activity at the plasma membrane was abolished, implicating cPKCs in the early phase of the PKC response. The effect is less dramatic at the Golgi, consistent with previous data that generally localizes the Ca^{2+}-independent nPKCs at the Golgi (7, 23). When intracellular Ca^{2+} was chelated, it was impossible to rescue the fast kinetics of the response by overexpressing PKCδ, indicating a genuine difference in the rate of activation of cPKCs *versus* nPKCs. Additionally, although inhibiting cPKCs reduced the rate of response, it did not block the later phase of activation, suggesting a role for the nPKCs in sustaining phosphorylation.

We determined conditions for intracellular Ca^{2+} elevation without the corresponding DAG production and used the localized reporters to test for cPKC activity. Although Ca^{2+} appears to be required for the faster kinetics of cPKCs, Ca^{2+} alone is not sufficient to drive activation of cPKCs in live cells, consistent with *in vitro* data (24). This data also underscores the importance of the feed forward effect of Ca^{2+} on PLC-mediated DAG generation (25, 26), since DAG must be generated along with inositol trisphosphate production in response to P2Y receptor stimulation; however, this amount of DAG is clearly not sufficient to be read out using our DAG reporter and is not sufficient to activate PKC at even the most responsive region, the plasma membrane.

PKC activity persisted longer at the Golgi than at the plasma membrane, which could not be explained by differences in phosphatase activity; however, regional variations in DAG production could cause differences in sustained phosphorylation by PKC. Previous methods for detecting whole cell DAG production consisted of imaging DAGR, a probe consisting of the entire C1 domain of PKCβ flanked by CFP and YFP. Upon generation of DAG, DAGR translocates to cellular membranes, and the increased concentration resulting from the reduction in dimensionality is read as an increase in intermolecular FRET (1). One disadvantage of DAGR is that it cannot be localized to any particular subset of cellular membranes, because targeting the reporter would confine the movement of DAGR, which is the sole basis for the FRET change.

In order to visualize local production of DAG, we transfected COS 7 cells with targeted FRET-based DAG reporters: PMDAGR and GolgiDAGR. Using the targeted DAGRs, we were able to correlate persistence of the PKC response with local DAG persistence. Specifically, DAG persistence and the corresponding PKC activity were highly sustained at the Golgi, whereas DAG and PKC activity at the plasma membrane reversed back to base line within 35 min. Competitively inhibiting PKC activation by overexpressing a DBD shortens the duration of the PKC response to UTP, further supporting the idea that DAG persistence is required for sustained PKC activity. However, overexpression of the DBD does not completely block the early phase of the PKC activation, probably due to the fast kinetics of the cPKC response imparted by the C2 domain.

A major finding from our study is that the Golgi is the site of the most robust and sustained activity of endogenous PKC in response to natural agonists. Specifically, we find that although the magnitude of initial PKC activation is similar at the plasma membrane, the historical site of PKC activation, and at the Golgi, the duration of the activity persists considerably longer at the Golgi. This activity is relatively insensitive to either Ca^{2+} chelation or inhibition by Gö6976, an inhibitor directed at cPKCs, suggesting that it is mediated by nPKCs. Consistent with this, biochemical fractionation, immunofluorescence, and green fluorescent protein fusion protein studies over the past decade have established that the novel isozymes of PKC (δ, ϵ, and θ) localize to intracellular membranes, most typically Golgi, following activation (*e.g.* see Refs. 7, 23, 27, 28, and 30–32). Taken together, our data show that the Golgi-localized PKC accounts for the bulk of the PKC activity following the first few minutes after G protein-coupled receptor stimulation. Our data also reveal that the plasma membrane is the site of the initial activation of PKC and that this activity is Ca^{2+}-driven and inhibited by Gö6976. This is consistent with the abundant literature showing that conventional isozymes of PKC (α, β, and γ) translocate to the plasma membrane following activation (*e.g.* see Refs. 9, 10, and 33–36).

Although DAG production at the Golgi has been demonstrated elegantly by indirect methods (37) and DAG-dependent binding of proteins at the Golgi has been established previously (38), this is the first imaging study directly visualizing stimulus-dependent DAG generation at the Golgi. We find that DAG is rapidly produced at this location and that, in striking contrast to plasma membrane DAG, the levels of this second messenger are sustained at the Golgi. DAG can be produced at the Golgi by several means, including phospholipase D-mediated hydrolysis of phosphatidylcholine to phosphatatidic acid, which is converted to DAG via phosphatidic acid phosphatase (39). PLC activity has also been documented to generate DAG at the Golgi. Specifically, PLCϵ translocates to the Golgi in a Ras-proximate 1 (Rap1)-dependent manner (40). Intriguingly, in response to G protein-coupled receptor agonists, it has recently been shown that PLCϵ is responsible for sustained (60-min) phosphoinositide hydrolysis, whereas PLCβ is responsible for acute (1-min) phosphoinositide hydrolysis (41). Thus, activation of PLCϵ could account for the sustained DAG levels at the Golgi.

In this study, cPKCs mediated rapid, transient phosphorylation, whereas phosphorylation mediated by nPKCs was slower and longer in duration. The fast phase was more prominent at the plasma membrane, and the slow phase was more persistent at the Golgi. Thus, in response to UTP, specific substrate phosphorylation was achieved by variation in the kinetics and duration of the PKC response resulting from recruitment of different isoforms to different regions. Because isoforms of the PKC family share a conserved kinase core and differ most in their regulatory modules (29), spatiotemporal specificity may be more important in determining PKC substrate specificity than active site specificity, underscoring the need for sensitive tools to study spatiotemporal dynamics of PKC signaling.

Acknowledgments—We thank Nathan Shaner for generating constructs targeting CKAR to the nucleus and cytosol, Roger Tsien for helpful discussions, and Jon Violin for critical reading of the manuscript.

REFERENCES

1. Violin, J. D., Zhang, J., Tsien, R. Y., and Newton, A. C. (2003) *J. Cell Biol.* **161,** 899–909
2. Vermeulen, K., Berneman, Z. N., and Van Bockstaele, D. R. (2003) *Cell Prolif.* **36,** 165–175
3. Naor, Z. (1990) *Endocr. Rev.* **11,** 326–353
4. Majumder, P. K., and Sellers, W. R. (2005) *Oncogene* **24,** 7465–7474
5. Newton, A. C. (2003) *Biochem. J.* **370,** 361–371
6. Orr, J. W., and Newton, A. C. (1992) *Biochemistry* **31,** 4661–4667
7. Giorgione, J. R., Lin, J. H., McCammon, J. A., and Newton, A. C. (2006) *J. Biol. Chem.* **281,** 1660–1669
8. Lamark, T., Perander, M., Outzen, H., Kristiansen, K., Overvatn, A., Michaelsen, E., Bjorkoy, G., and Johansen, T. (2003) *J. Biol. Chem.* **278,** 34568–34581
9. Oancea, E., and Meyer, T. (1998) *Cell* **95,** 307–318
10. Sakai, N., Sasaki, K., Ikegaki, N., Shirai, Y., Ono, Y., and Saito, N. (1997) *J. Cell Biol.* **139,** 1465–1476
11. Wang, Q. J., Bhattacharyya, D., Garfield, S., Nacro, K., Marquez, V. E., and Blumberg, P. M. (1999) *J. Biol. Chem.* **274,** 37233–37239
12. Wang, W. L., Yeh, S. F., Chang, Y. I., Hsiao, S. F., Lian, W. N., Lin, C. H., Huang, C. Y., and Lin, W. J. (2003) *J. Biol. Chem.* **278,** 37705–37712
13. Fulton, D., Babbitt, R., Zoellner, S., Fontana, J., Acevedo, L., McCabe, T. J., Iwakiri, Y., and Sessa, W. C. (2004) *J. Biol. Chem.* **279,** 30349–30357
14. Kanaji, S., Iwahashi, J., Kida, Y., Sakaguchi, M., and Mihara, K. (2000) *J. Cell Biol.* **151,** 277–288
15. Sasaki, K., Sato, M., and Umezawa, Y. (2003) *J. Biol. Chem.* **278,** 30945–30951
16. Wen, W., Meinkoth, J. L., Tsien, R. Y., and Taylor, S. S. (1995) *Cell* **82,** 463–473
17. Makkerh, J. P., Dingwall, C., and Laskey, R. A. (1996) *Curr. Biol.* **6,** 1025–1027
18. Castagna, M., Takai, Y., Kaibuchi, K., Sano, K., Kikkawa, U., and Nishizuka, Y. (1982) *J. Biol. Chem.* **257,** 7847–7851
19. Balboa, M. A., Firestein, B. L., Godson, C., Bell, K. S., and Insel, P. A. (1994) *J. Biol. Chem.* **269,** 10511–10516
20. Insel, P. A., Ostrom, R. S., Zambon, A. C., Hughes, R. J., Balboa, M. A., Shehnaz, D., Gregorian, C., Torres, B., Firestein, B. L., Xing, M., and Post, S. R. (2001) *Clin. Exp. Pharmacol. Physiol.* **28,** 351–354
21. Grynkiewicz, G., Poenie, M., and Tsien, R. Y. (1985) *J. Biol. Chem.* **260,** 3440–3450
22. Harrison, S. M., and Bers, D. M. (1987) *Biochim. Biophys. Acta* **925,** 133–143
23. Kajimoto, T., Shirai, Y., Sakai, N., Yamamoto, T., Matsuzaki, H., Kikkawa, U., and Saito, N. (2004) *J. Biol. Chem.* **279,** 12668–12676
24. Hannun, Y. A., Loomis, C. R., and Bell, R. M. (1985) *J. Biol. Chem.* **260,** 10039–10043
25. Murthy, K. S., Zhou, H., Huang, J., and Pentyala, S. N. (2004) *Am. J. Physiol.* **287,** C1679–C1687
26. Thore, S., Dyachok, O., Gylfe, E., and Tengholm, A. (2005) *J. Cell Sci.* **118,** 4463–4471
27. Lehel, C., Olah, Z., Jakab, G., and Anderson, W. B. (1995) *Proc. Natl. Acad. Sci. U. S. A.* **92,** 1406–1410
28. England, K., and Rumsby, M. G. (2000) *Biochem. J.* **352,** 19–26
29. Nishikawa, K., Toker, A., Johannes, F. J., Songyang, Z., and Cantley, L. C. (1997) *J. Biol. Chem.* **272,** 952–960
30. Kang, M., and Walker, J. W. (2005) *J. Mol. Cell Cardiol.* **38,** 753–764
31. Kashiwagi, K., Shirai, Y., Kuriyama, M., Sakai, N., and Saito, N. (2002) *J. Biol. Chem.* **277,** 18037–18045
32. Schultz, A., Jonsson, J. I., and Larsson, C. (2003) *Cell Death Differ.* **10,** 662–675
33. Ohmori, S., Sakai, N., Shirai, Y., Yamamoto, H., Miyamoto, E., Shimizu, N., and Saito, N. (2000) *J. Biol. Chem.* **275,** 26449–26457
34. Saito, K., Ito, E., Takakuwa, Y., Tamura, M., and Kinjo, M. (2003) *FEBS Lett.* **541,** 126–131
35. Abdel-Raheem, I. T., Hide, I., Yanase, Y., Shigemoto-Mogami, Y., Sakai, N., Shirai, Y., Saito, N., Hamada, F. M., El-Mahdy, N. A., Elsisy Ael, D., Sokar, S. S., and Nakata, Y. (2005) *Br. J. Pharmacol.* **145,** 415–423
36. Dale, L. B., Babwah, A. V., Bhattacharya, M., Kelvin, D. J., and Ferguson, S. S. (2001) *J. Biol. Chem.* **276,** 35900–35908
37. Baron, C. L., and Malhotra, V. (2002) *Science* **295,** 325–328
38. Carrasco, S., and Merida, I. (2004) *Mol. Biol. Cell* **15,** 2932–2942
39. Billah, M. M., and Anthes, J. C. (1990) *Biochem. J.* **269,** 281–291
40. Song, C., Hu, C-D., Masago, M., Kariya, K., Yamawaki-Kataoka, Y., Shibatohge, M., Wu, D., Satoh, T., and Kataoka, T. (2001) *J. Biol. Chem.* **276,** 2752–2757
41. Kelley, G. G., Kaproth-Joslin, K. A., Reks, S. E., Smrcka, A. V., and Wojcikiewicz, R. J. H. (2006) *J. Biol. Chem.* **281,** 2639–2648